



Hierarchical bimetal embedded in carbon nanoflower electrocatalysts derived from metal-organic frameworks for efficient oxygen evolution reaction

Panpan He ^{a,1}, Yuhang Wu ^{a,1}, Hongxu Chen ^a, Zhenwang Zhu ^a, Huajian Liu ^a,
Junkuo Gao ^{a,*}, Hui Xu ^{b,*}

^a Institute of Fiber Based New Energy Materials, The Key Laboratory of Advanced Textile Materials and Manufacturing Technology of Ministry of Education, School of Materials Science and Engineering, Zhejiang Sci-Tech University, Hangzhou, 310018, China

^b College of Materials Science and Engineering, China Jiliang University, Hangzhou, 310018, PR China



ARTICLE INFO

Article history:

Received 11 July 2019

Received in revised form

4 September 2019

Accepted 6 September 2019

Available online 6 September 2019

Keywords:

Metal-organic frameworks

Nanoflower

Core@shell structure

Metal–carbon composite

Oxygen evolution reaction

Electrocatalysis

ABSTRACT

Developing high-performance and cost-effective electrocatalysts for oxygen evolution reaction (OER) is crucial to renewable energy conversion and storage technologies. Herein, bimetallic N-doped carbon electrocatalysts with various morphologies are derived from Hofmann-type metal-organic frameworks by carbonization and oxidization. Notably, the flower-like nano-catalyst FeNi@OCNF exhibits core@shell structure, hierarchical pore network and large specific surface area ($331.3 \text{ m}^2 \text{ g}^{-1}$), leading to tunable electronic structure, efficient mass transfer as well as abundant exposed active sites. Moreover, the formative FeC_x , NiO and FeNi bimetal mutually optimize electronic structure of graphitic layer, conducting to high property. FeNi @OCNF demonstrates an excellent OER performance with a low overpotential of 281 mV at 10 mA cm^{-2} , significantly outperforming the other catalyst CoNi @OCNP (373 mV) and commercial IrO_2 (308 mV), and also owns long-term stability. The result may inspire more design of MOF-derived catalysts with multiscale structures and multi-components for various electrochemical energy conversion devices.

© 2019 Elsevier B.V. All rights reserved.

1. Introduction

To meet the challenges of fossil energy depletion and triggered environmental pollution, considerable efforts have been devoted to developing renewable energy conversion and storage technologies [1–3]. Essentially, the oxygen evolution reaction (OER) is a cornerstone of innovative technologies such as water electrolysis, metal-air batteries and reversible fuel cells [4–6]. However, the sluggish four-electron process of OER exhibits high overpotential and low reaction rate, resulting in unsatisfied energy transfer efficiency [7–10]. Currently, noble metal oxides such as IrO_2 and RuO_2 exhibit prominent OER catalytic property, while the scarcity, expensiveness and instability hinder their further application [11–13]. Therefore, alternative catalysts with low cost and high

performance are great demands.

Complicated nanostructure is a key indicator of high catalytic performance. Unique constructions such as core@shell structures [14], hollow structures [15], nanoflowers [16] and multilevel structures [17] are widely applied in electrocatalytic field, which thanks to the large specific surface area, uniform dispersion of active sites, as well as high mechanical/chemical stability. Besides, nanoporous structures not only expose vast active sites, but also facilitate the penetration/diffusion of electrolyte and release of O_2 , thus accelerate mass transfer [18]. On the other hand, the earth-abundant transition metal and derivative have shown enormous OER catalytic potential [19]. For instance, metal oxides NiO and Co_3O_4 exhibit comparable activity with noble metals [20], and metal carbide Fe_3C has shown ability for OER [21]. Besides, bimetal compound such as FeNi reveals superior activity due to coupling effect [22]. Furthermore, it is an available strategy to embed metal nanoparticles into carbon shells to form metal–carbon composites, thus achieve additional host-guest synergic effect and high catalysis stability [23–25]. Therefore, synthesizing bimetal oxide/

* Corresponding author.

** Corresponding author.

E-mail addresses: jkgao@zstu.edu.cn (J. Gao), huixu@cjlu.edu.cn (H. Xu).

¹ These authors contributed equally to this paper.

carbide@carbon composite with multiscale porous structure is an advisable way to achieve notable electrocatalysts.

Metal-organic frameworks (MOFs), as a family of crystalline porous materials, are the ideal precursors to prepare remarkable electrocatalysts [26–31]. Firstly, MOFs are constructed with metal centers and organic linkers, which can ideally transfer to customized metal–carbon composites by high-temperature pyrolysis. Secondly, metal species can promote the degree of graphitization, while the carbon layers keep metal nanoparticles from aggregation [32], which result in high conductivity and uniform dispersion of active sites. Moreover, MOFs derivatives can inherit unique nanostructure from templates, and form hierarchical pore network [33], which expose more active sites and accelerate the mass transfer.

Herein, we innovatively reported two excellent bimetallic electrocatalysts (FeNi@OCNF and CoNi@OCNP) derived from MOFs precursors (illustrated in **Scheme 1**). The catalysts show different morphologies which notably influence the OER performance. FeNi@OCNF exhibits rose-like nanostructure subtly composed of core@shell and hollow structures, contributing to uniform dispersion of active sites, optimized electronic structure, and high stability. The unique pore size distribution also accelerates the diffusion of reactants and release of O_2 bubbles, leading to more efficient mass transfer. Moreover, the formation of metal oxides/carbides, nitrogen doping and synergy mechanism of FeNi bimetal mutually boom the OER activity. As a result, the optimized FeNi@OCNF exhibits a better performance with an overpotential of 281 mV (10 mA cm^{-2}) and a Tafel slope of 36 mV dec^{-1} , preceding the commercial IrO_2 electrocatalyst, and also shows excellent long-term durability.

2. Results and discussion

The synthesis process of FeNi@OCNF is illustrated in **Scheme 1** (as for CoNi@OCNP, replace Fe^{2+} with Co^{2+}) and minutely described in the experimental section (supporting information). Primarily, bimetal ions coordinate with CN^- and pyridine to form MOFs template $\text{M}(\text{py})_2[\text{Ni}(\text{CN})_4]$ (M refers to $\text{Fe}^{2+}/\text{Co}^{2+}$), while adding surfactant PVP aims to control distinct morphologies [34]. The X-ray diffraction (XRD) patterns of the Hofmann MOFs were supported in **Fig. S1**, matched with the simulated curve. Subsequently, MOFs were pyrolyzed at 800°C under N_2 atmosphere to obtain metal–carbon composites, and $0.5 \text{ M H}_2\text{SO}_4$ was used to remove unstable metal species from surface. The ultima catalysts were acquired by 350°C oxidation, which formed available metal oxides.

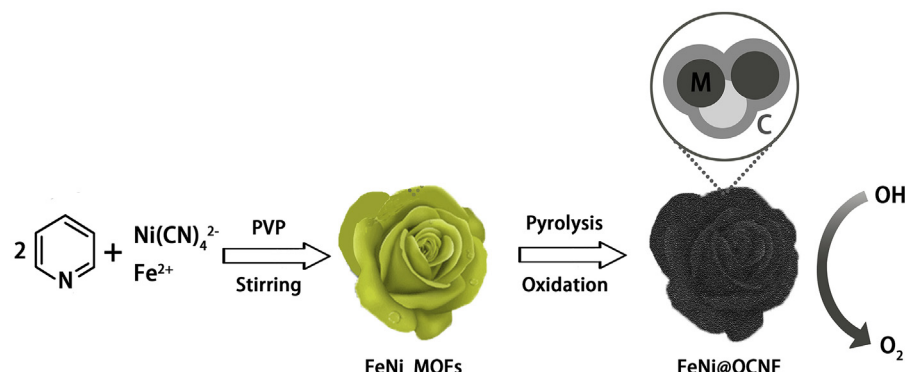
The morphologies of FeNi@OCNF and CoNi@OCNP were investigated by scanning electron microscope (SEM). As shown in **Fig. 1a** and **e**, two precursors exhibited dramatically different

morphologies. FeNi-MOFs showed a rose flower-like construction with a diameter around 800 nm, which was assembled by a dozen petals with thicknesses about 100 nm. Whereas CoNi-MOFs presented as nanoparticles with size of about 150 nm, which partly reunited. As **Fig. 1b** displays, after pyrolysis and oxidation, FeNi@OCNF inherited the complicated nanoflower morphology, and also acquired rough and porous surface, which contribute to additional exposed sites and fast diffusion of electrolyte [35]. However, CoNi@OCNP aggregated together after annealing, with metal nanoparticles dispersed irregularly, as **Fig. 1f** shows.

Transmission electron microscope (TEM) was conducted to further investigate the construction of catalysts. As **Fig. 1c** and **d** shows, FeNi@OCNF nanoflower was composed of tiny core@shell cells as well as hollow structures. The metal nanoparticle cores ($10\text{--}20 \text{ nm}$) were encapsulated in spherical graphite shells ($5\text{--}10 \text{ nm}$), which availably protect the metal species from electrolyte corrosion and self-aggregation [36,37]. Additionally, the hollow nanostructures with low density and thin shells provide extra triple-phase interface and ensure high permeation of reactant [38]. Nevertheless, as shown in **Fig. 1g** and **h**, CoNi@OCNP nanoparticles exhibited ruleless organization, for which metal particles ($10\text{--}20 \text{ nm}$) were imperfectly wrapped by carbon layers. The HRTEM in **Fig. S3** exposed the (002) plane of graphitic carbon in both catalysts, (220) plane of Co_3O_4 in CoNi@OCNP, and (010) plane of FeC_x in FeNi@OCNF, respectively. Moreover, energy dispersive X-ray spectroscopy (EDS) elemental mapping was conducted to exam the elemental distribution of FeNi@OCNF. As shown in **Fig. 1i-l**, Fe, Ni and O were uniformly dispersed in cores, while appropriate distance was maintained between cores, which lead to synergistic effect between metal/oxides and carbon shells. The large distribution of C and N can be clearly observed in **Fig. S4**.

The X-ray diffraction (XRD) patterns of electrocatalysts were shown in **Fig. 2**, confirming the presence of metal/metal oxide/metal carbide composition. For FeNi@OCNF, the peak located at about 26° is assigned to (002) plane of graphitic C (PDF#75–1621), while diffraction peaks at 35.9° and 43.9° are attributed to (010) and (111) planes of FeC_x alloy (PDF#03–0400), which are consistent with the HRTEM data above mentioned. The peak at 37.2° can be indexed as (101) plane of NiO species (PDF#44–1159). While for CoNi@OCNP, no obvious graphitic peak was found, implying the poorer crystalline of graphite C. The main peaks at 31.3° , 37.0° , 43.3° and 44.2° , are respectively indexed to (220) and (311) planes of Co_3O_4 (PDF#74–1656), (012) plane of NiO (PDF#44–1159), and (111) plane of cubic Co (PDF#15–0806). It's well known that Co_3O_4 and NiO demonstrate the comparable OER activity with precious metals [20].

The surface chemical properties of FeNi@OCNF were further dissected by X-ray photoelectron spectroscopy (XPS), which



Scheme 1. An illustration of the fabrication of FeNi@OCNF (Oxydic Carbon NanoFlowers).

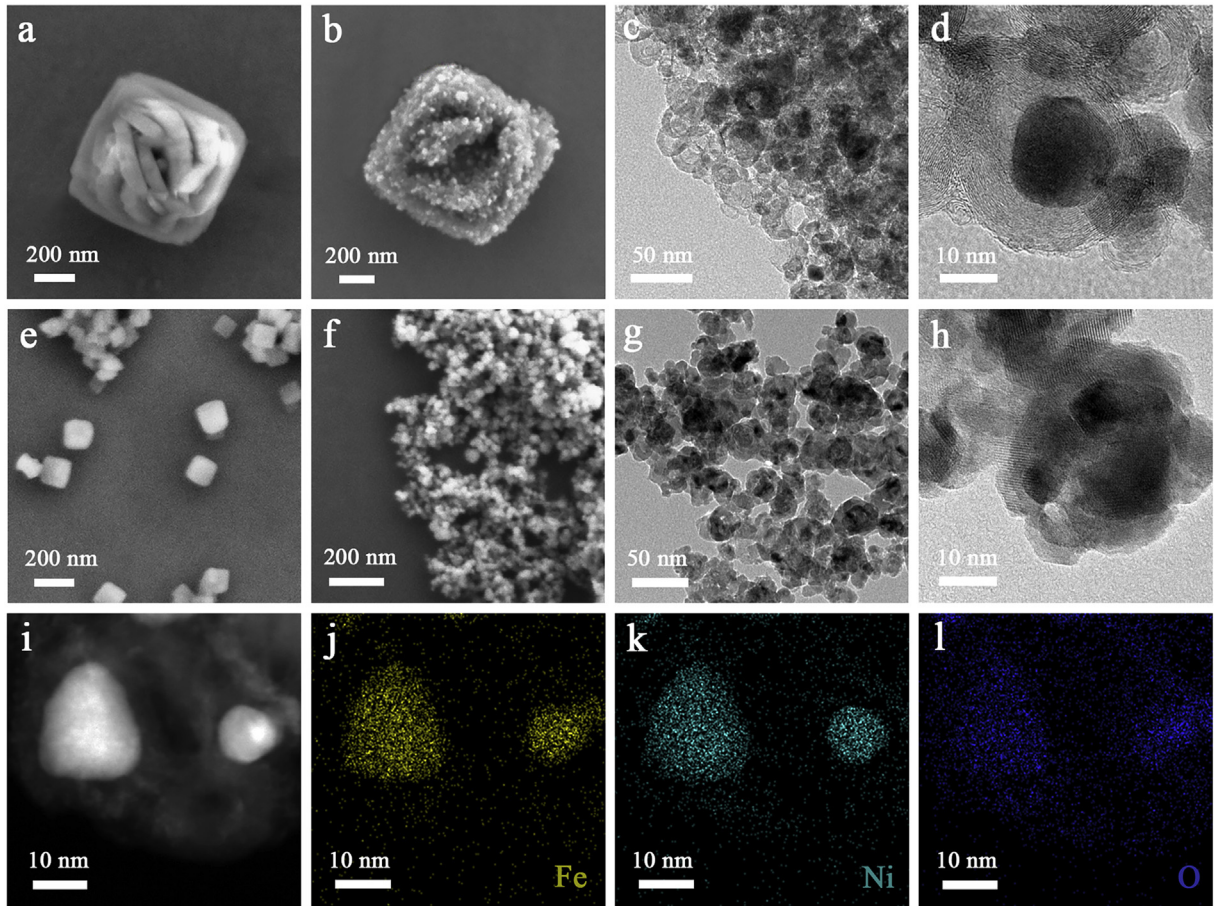


Fig. 1. SEM images of (a) FeNi-MOFs, (b) FeNi@OCNF, (e) CoNi-MOFs, (f) CoNi@OCNP; TEM images of (c-d) FeNi@OCNF, (g-h) CoNi@OCNP; EDS mappings of FeNi@OCNF (i) HAADF image, (j-l) elemental mappings of Fe, Ni and O.

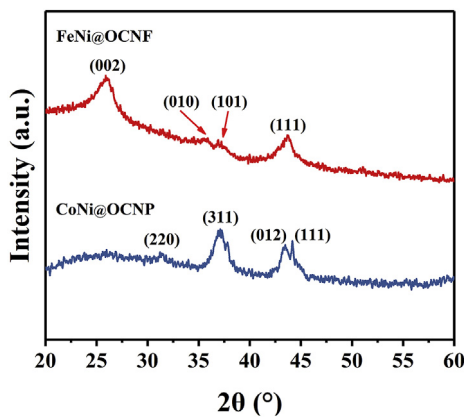


Fig. 2. The XRD patterns of FeNi@OCNF and CoNi@OCNP.

revealed the presence of Fe (0.77%), Ni (2.23%), O (13.09%), N (4.75%) and C (79.16%). The slightly detected content of Fe and Ni confirmed that metal species were well encapsulated by carbon shells. As shown in Fig. 3a, the Fe 2p spectrum exhibited Fe 2p_{1/2} and Fe 2p_{3/2} peaks respectively. The Fe 2p_{3/2} can be deconvoluted to Fe²⁺ and Fe³⁺ oxidation state at 710.0 and 712.3 eV, and the peaks at 724.0 and 725.4 eV account for the Fe²⁺ 2p_{1/2} and Fe³⁺ 2p_{1/2} [16], which can be attributed to the formation of oxides and carbides. The fitted peaks of Ni²⁺ (situated at 854.5 and 872.3 eV) are due to

NiO species, and the peak at 855.9 eV is ascribed to Ni³⁺ [39], along with two satellite peaks at 861.0 and 878.7 eV. As shown in Fig. 3c, the deconvolution of O 1s spectrum declared the existence of metal-oxygen bond (529.3 eV), oxygen vacancy (530.75 eV) and carbon-oxygen bond (532.6 eV) [40,41], in which the oxygen vacancy was dominant. Oxygen vacancy is known to promote the conductivity of catalysts [42]. Furthermore, the peaks of N 1s located at 398.1, 399.5 and 401.0 eV corresponded to pyridinic N, pyrrolic N and graphitic N respectively [43,44]. Previous study has confirmed that most nitrogen dopants especially pyridinic N contribute to electrocatalytic activity [20]. As shown in Fig. S5, the binding energies of C–C and C–N shifted negatively to 283.8 and 284.6 eV, which indicated that electronic structure of carbon layer was modulated by iron doping [45]. Consequently, the heteroatom and optimized carbon frameworks mutually promoted the charge transfer efficiency.

The pore structure and specific surface area are essential to performance, which were characterized by BET method. As shown in Fig. 4, a typical type-IV sorption isotherm with overt hysteresis loop indicates the well-developed micro/mesoporous in FeNi@OCNF [36]. Furthermore, the nested figure showed hierarchical distribution of pore sizes (mainly at 2.64 nm and 11.24 nm), which not only facilitated the permeation and adsorption of ions, but also prevented O₂ bubbles blocking channels, thus leading to efficient mass transfer [20,46]. Besides, FeNi@OCNF possessed ultrahigh specific surface area (331.3 m² g⁻¹) as well as large pore volume (0.882 cm³ g⁻¹), contributing to more accessible sites.

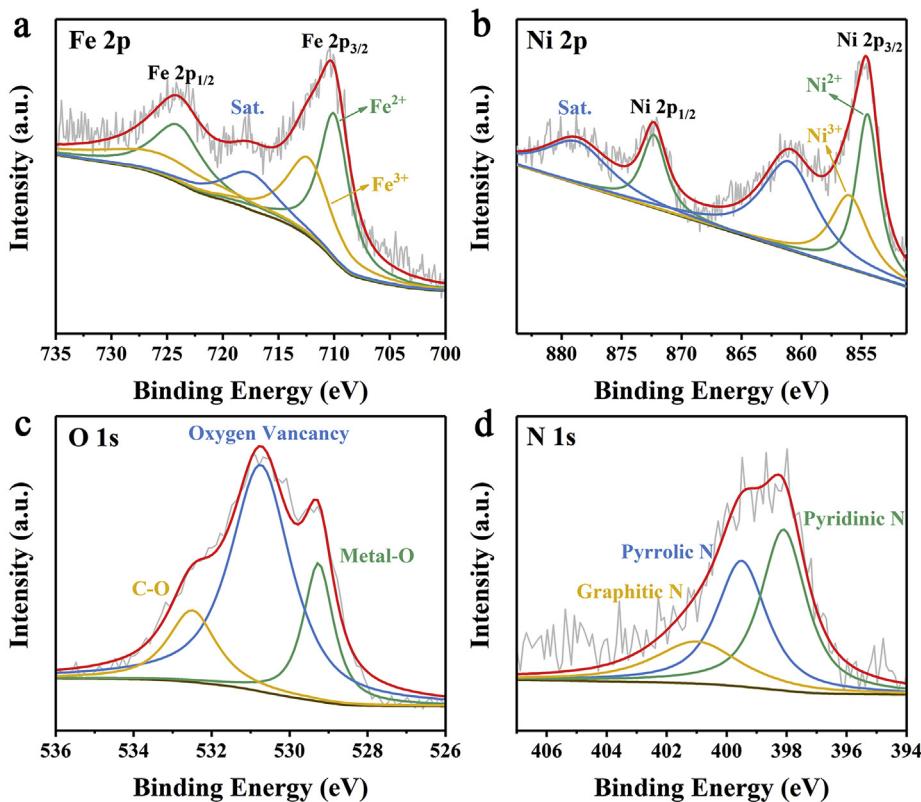


Fig. 3. XPS spectra of FeNi@OCNF (a) Fe 2p, (b) Ni 2p, (c) O 1s, (d) N 1s.

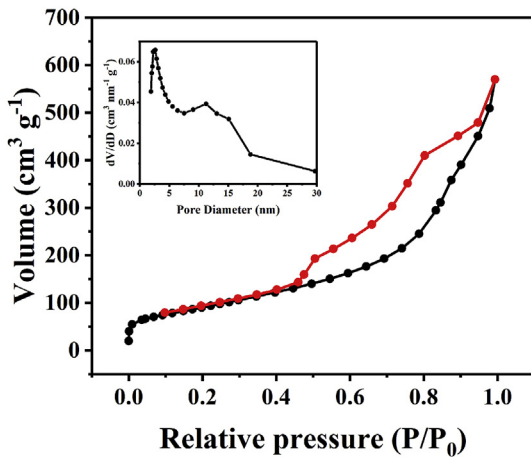


Fig. 4. The nitrogen sorption isotherm and pore size distribution curve of FeNi@OCNF.

However, as supported in Fig. S6, CoNi@OCNP merely owned featureless pore structures, low specific area ($71.3 \text{ m}^2 \text{ g}^{-1}$) and pore volume ($0.586 \text{ cm}^3 \text{ g}^{-1}$), showing weak competitiveness with FeNi@OCNF.

The OER performance of bimetallic catalysts was tested in 1 M KOH using glass carbon electrode (GCE) as working electrode. The linear sweep voltammetry (LSV) was conducted to gain polarization curves of catalysts with 90% iR compensation. As shown in Fig. 5a, the overpotentials of FeNi@OCNF, CoNi@OCNP and commercial IrO₂ at 10 mA cm^{-2} are 281 mV, 373 mV, 308 mV respectively. Notably, FeNi@OCNF shows an ultra-low overpotential which is superior to IrO₂ and most OER catalysts (Table S1) [47]. When the current density is larger than 46 mA cm^{-2} , CoNi@OCNP

requires a lower overpotential than IrO₂, indicating its catalysis advantage in high current density area. The metal oxide might be a contributor to the performance, because the overpotential of both catalysts decreased sharply after oxidation (supported in Fig. S7). The electrocatalytic kinetics was further investigated by Tafel slope, which was based on polarization curve. The Tafel slope of FeNi@OCNF (36 mV dec^{-1}) is smaller than that of IrO₂ (40 mV dec^{-1}) and CoNi@OCNP (75 mV dec^{-1}), confirming its distinguished property. Moreover, electrochemical impedance spectroscopy (EIS) was conducted to evaluate the charge transfer resistance (R_{ct}) of catalysts. As Fig. 5c shows, FeNi@OCNF owns a much smaller Nyquist semicircle than CoNi@OCNP, indicating the small R_{ct} of FeNi catalyst. The electronic structure of graphitic layers can be effectively optimized by encapsulated FeNi bimetal as well as FeC_x alloy, which leads to both efficient interfacial electron transfer and high conductance [45,48]. Synthetically, FeNi@OCNF has a much better OER activity than CoNi@OCNP, which thanks to its intricate nanoflower morphology, hierarchical pore structure, and tunable electronic structure. Furthermore, the long-time stability is a crucial indicator for practical application. Fig. 5d showed the chronopotentiometry curve of FeNi@OCNF tested at a constant current density (10 mA cm^{-2}). The voltage maintained well after continuous working for 12 h, implying the excellent durability. The spherical carbon shell could protect the metal nanoparticles from electrolyte corrosion [5], and Fe–C bonds further stabilizes the metal species [20], resulting in high stability. The morphology of FeNi@OCNF after persistent operation remained well (Fig. S8), confirming the structure stability of nanoflower.

3. Conclusion

To sum up, we successfully synthesized two MOF-derived

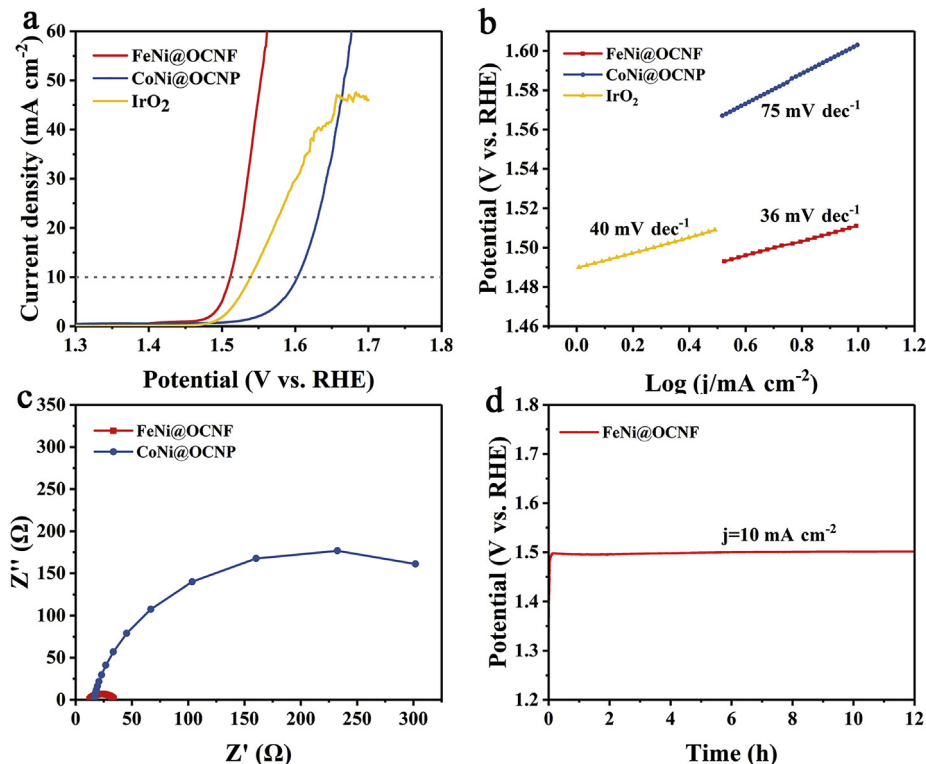


Fig. 5. (a) Linear sweep voltammetry (LSV) curves of FeNi@OCNF, CoNi@OCNP and IrO₂ at a scan rate of 5 mV s⁻¹. (b) Tafel slope plots of FeNi@OCNF, CoNi@OCNP and IrO₂. (c) Nyquist plots of FeNi@OCNF, CoNi@OCNP at a potential of 1.544 V. (d) Chronopotentiometric test (V-t curve) of FeNi@OCNF for 12 h.

electrocatalysts with distinct morphologies through a available pyrolysis-oxidation strategy. Remakably, FeNi@OCNF shows a excellent OER activity with an overpotential of 281 mV at 10 mA cm⁻², notably preceding CoNi@OCNP (373 mV) and commercial IrO₂ (308 mV), also demonstrates long-time stability in alkaline media. The nanoflower and core@shell structures, hierarchical pore network and large specific area (331.1 m² g) contribute to abundant exposed sites, high stability and efficient mass transfer. While the formation of metal oxides/carbides as well as FeNi bimetal synergistic effect signally activate neighboring N-doped carbon shells, leading to high electrochemical activity. The present study will inspire more design of MOF-derived catalysts with intricate structures for various energy conversion and storage technologies, such as metal-air batteries and reversible fuel cells.

Acknowledgements

This work was supported by the National Natural Science Foundation of China (51602301 and 51672251) and the Fundamental Research Funds of Zhejiang Sci-Tech University (2019Q007).

Appendix A. Supplementary data

Supplementary data to this article can be found online at <https://doi.org/10.1016/j.jallcom.2019.152192>.

References

- [1] Z. Liang, R. Zhao, T. Qiu, R. Zou, Q. Xu, Metal-organic framework-derived materials for electrochemical energy applications, *Inside Energy* 1 (2019) 100001.
- [2] C. Li, H. Xu, J. Gao, W. Du, L. Shangguan, X. Zhang, R. Lin, H. Wu, W. Zhou, X. Liu, J. Yao, B. Chen, Tunable titanium metal-organic frameworks with infinite 1D Ti-O rods for efficient visible-light-driven photocatalytic H₂ evolution, *J. Mater. Chem. A* 7 (2019) 11928–11933.
- [3] T. Wu, M. Pi, X. Wang, W. Guo, D. Zhang, S. Chen, Developing bifunctional electrocatalyst for overall water splitting using three-dimensional porous Co₃ nanospheres integrated on carbon cloth, *J. Alloy. Comp.* 729 (2017) 203–209.
- [4] D. Chen, C. Dong, Y. Zou, D. Su, Y. Huang, L. Tao, S. Dou, S. Shen, S. Wang, In situ evolution of highly dispersed amorphous CoOx clusters for oxygen evolution reaction, *Nanoscale* 9 (2017) 11969–11975.
- [5] X. Zheng, Y. Cao, D. Liu, M. Cai, J. Ding, X. Liu, J. Wang, W. Hu, C. Zhong, Bimetallic metal-organic-framework/reduced graphene oxide composites as bifunctional electrocatalysts for rechargeable Zn-air batteries, *ACS Appl. Mater. Interfaces* 11 (2019) 15662–15669.
- [6] S. Dresp, P. Strasser, Non-noble metal oxides and their application as bifunctional catalyst in reversible fuel cells and rechargeable air batteries, *ChemCatChem* 10 (2018) 4162–4171.
- [7] B. You, Y. Sun, Innovative strategies for electrocatalytic water splitting, *Acc. Chem. Res.* 51 (2018) 1571–1580.
- [8] Z. Seh, J. Kibsgaard, C. Dickens, I. Chorkendorff, J. Norskov, T. Jaramillo, Combining theory and experiment in electrocatalysis: insights into materials design, *Science* 355 (2017) eaad4998.
- [9] X. Li, T. Wang, C. Wang, An advanced flower-like Co-Ni/PI-CNT film electrocatalyst for oxygen evolution reaction, *J. Alloy. Comp.* 729 (2017) 19–26.
- [10] X. Hao, Z. Jiang, X. Tian, X. Hao, T. Maiyalagan, Z. Jiang, A novel particle-in-nanoplate architecture of iron nickel phosphide intertwined with carbon nanotubes for efficient water oxidation and high-performance sodium-ion batteries, *J. Alloy. Comp.* 791 (2019) 1220–1230.
- [11] K. Zhu, X. Zhu, W. Yang, Application of in situ techniques for the characterization of NiFe-based oxygen evolution reaction (OER) electrocatalysts, *Angew. Chem. Int. Ed.* 58 (2019) 1252–1265.
- [12] Y. Jiao, Y. Zheng, M. Jaroniec, S. Qiao, Design of electrocatalysts for oxygen- and hydrogen-involving energy conversion reactions, *Chem. Soc. Rev.* 44 (2015) 2060–2086.
- [13] H. Si, Q. Deng, L. Chen, L. Wang, X. Liu, W. Wu, Y. Zhang, J. Zhou, H. Zhang, Hierarchical graphdiyne@NiFe layered double hydroxide heterostructures as a bifunctional electrocatalyst for overall water splitting, *J. Alloy. Comp.* 794 (2019) 261–267.
- [14] Y. Pan, K. Sun, S. Liu, X. Cao, K. Wu, W. Cheong, Z. Chen, Y. Wang, Y. Li, Y. Liu, D. Wang, Q. Peng, C. Chen, Y. Li, Core-shell ZIF-8@ZIF-67-derived CoP nanoparticle-embedded N-doped carbon nanotube hollow polyhedron for efficient overall water splitting, *J. Am. Chem. Soc.* 140 (2018) 2610–2618.
- [15] B. Xia, Y. Yan, N. Li, H. Wu, X. Lou, X. Wang, A metal-organic framework-derived bifunctional oxygen electrocatalyst, *Nat. Energy* 1 (2016) 15006.
- [16] Y. Li, M. Lu, Y. Wu, H. Xu, J. Gao, J. Yao, Trimetallic metal-organic framework

- derived carbon-based nanoflower electrocatalysts for efficient overall water splitting, *Adv. Mater. Interfaces* 6 (2019) 1900290.
- [17] H. Xu, Z. Shi, Y. Tong, G. Li, Porous microrod arrays constructed by carbon-confined NiCo@NiCoO₂ core@shell nanoparticles as efficient electrocatalysts for oxygen evolution, *Adv. Mater.* 30 (2018) 1705442.
- [18] J. Feng, S. Ye, H. Xu, Y. Tong, G. Li, Design and synthesis of FeOOH/CeO₂ heterolayered nanotube electrocatalysts for the oxygen evolution reaction, *Adv. Mater.* 28 (2016) 4698–4703.
- [19] F. Lu, M. Zhou, Y. Zhou, X. Zeng, First-row transition metal based catalysts for the oxygen evolution reaction under alkaline conditions: basic principles and recent advances, *Small* 13 (2017) 1701931.
- [20] B. Zhu, D. Xia, R. Zou, Metal-organic frameworks and their derivatives as bifunctional electrocatalysts, *Coord. Chem. Rev.* 376 (2018) 430–448.
- [21] L. Wei, H. Sun, T. Yang, S. Deng, M. Wu, Z. Li, Iron carbide encapsulated by porous carbon nitride as bifunctional electrocatalysts for oxygen reduction and evolution reactions, *Appl. Surf. Sci.* 439 (2018) 439–446.
- [22] H. Tao, Y. Xu, X. Huang, J. Chen, L. Pei, J. Zhang, J. Chen, B. Liu, A general method to probe oxygen evolution intermediates at operating conditions, *Joule* 3 (2019) 1498–1509.
- [23] Z. Wang, S. Xiao, Z. Zhu, X. Long, X. Zheng, X. Lu, S. Yang, Cobalt-embedded nitrogen doped carbon nanotubes: a bifunctional catalyst for oxygen electrode reactions in a wide pH range, *ACS Appl. Mater. Interfaces* 7 (2015) 4048–4055.
- [24] J. Wang, H. Wu, D. Gao, S. Miao, G. Wang, X. Bao, High-density iron nanoparticles encapsulated within nitrogen-doped carbon nanoshell as efficient oxygen electrocatalyst for zinc-air battery, *Nano Energy* 13 (2015) 387–396.
- [25] Q. Wang, Y. Lei, Z. Chen, N. Wu, Y. Wang, B. Wang, Y. Wang, Fe/Fe₃C@C nanoparticles encapsulated in N-doped graphene-CNTs framework as an efficient bifunctional oxygen electrocatalyst for robust rechargeable Zn-air batteries, *J. Mater. Chem. A* 6 (2018) 516–526.
- [26] Y. Wang, W. Wu, Y. Rao, Z. Li, N. Tsubaki, M. Wu, Cation modulating electrocatalyst derived from bimetallic metal-organic frameworks for overall water splitting, *J. Mater. Chem. A* 5 (2017) 6170–6177.
- [27] A. Jayakumar, R. Antony, J. Zhao, J. Lee, MOF-derived nickel and cobalt metal nanoparticles in a N-doped coral shaped carbon matrix of coconut leaf sheath origin for high performance supercapacitors and OER catalysis, *Electrochim. Acta* 265 (2018) 336–347.
- [28] S. Dang, Q. Zhu, Q. Xu, Nanomaterials derived from metal-organic frameworks, *Nat. Rev. Mater.* 3 (2017) 17075.
- [29] B. Liu, H. Shioyama, T. Akita, Q. Xu, Metal-organic framework as a template for porous carbon synthesis, *J. Am. Chem. Soc.* 130 (2008) 5390–5391.
- [30] Y. Wei, M. Zhang, M. Kitta, Z. Liu, S. Horike, Q. Xu, A single-crystal open-capsule metal-organic framework, *J. Am. Chem. Soc.* 141 (2019) 7906–7916.
- [31] L. Wang, H. Xu, J. Gao, J. Yao, Q. Zhang, Recent progress in metal-organic frameworks-based hydrogels and aerogels and their applications, *Coord. Chem. Rev.* 398 (2019) 213016.
- [32] L. Zhang, J. Xiao, H. Wang, M. Shao, Carbon-based electrocatalysts for hydrogen and oxygen evolution reactions, *ACS Catal.* 7 (2017) 7855–7865.
- [33] Q. Zhu, W. Xia, T. Akita, R. Zou, Q. Xu, Metal-organic framework-derived honeycomb-like open porous nanostructures as precious-metal-free catalysts for highly efficient oxygen electroreduction, *Adv. Mater.* 28 (2016) 6391.
- [34] J. Gao, J. Cong, Y. Wu, L. Sun, J. Yao, B. Chen, Bimetallic hofmann-type metal-organic framework nanoparticles for efficient electrocatalysis of oxygen evolution reaction, *ACS Appl. Energy Mater.* 1 (2018) 5140–5144.
- [35] Y. Luo, L. Tang, U. Khan, Q. Yu, H. Cheng, X. Zou, B. Liu, Morphology and surface chemistry engineering toward pH-universal catalysts for hydrogen evolution at high current density, *Nat. Commun.* 10 (2019) 269.
- [36] J. Cong, H. Xu, M. Lu, Y. Wu, Y. Li, P. He, J. Gao, J. Yao, S. Xu, Two-dimensional Co@N-carbon nanocomposites facilely derived from metal-organic framework nanosheets for efficient bifunctional electrocatalysis, *Chem. Asian J.* 13 (2018) 1485–1491.
- [37] Y. Wu, M. Lu, Y. Li, P. He, S. Maddine, J. Gao, J. Yao, Folic acid derived bimetallic-doped hollow carbon nanostructures for efficient electrocatalytic oxygen evolution, *Chem. Asian J.* 13 (2018) 3274–3280.
- [38] S. Liu, Z. Wang, S. Zhou, F. Yu, M. Yu, C. Chiang, W. Zhou, J. Zhao, J. Qiu, Metal-organic-framework-derived hybrid carbon nanocages as a bifunctional electrocatalyst for oxygen reduction and evolution, *Adv. Mater.* 29 (2017) 1700874.
- [39] B. You, N. Jiang, M. Sheng, M. Bhushan, Y. Sun, Hierarchically porous urchin-like Ni₂P superstructures supported on nickel foam as efficient bifunctional electrocatalysts for overall water splitting, *ACS Catal.* 6 (2016) 714–721.
- [40] N. Zhang, S. Ruan, J. Han, Y. Yin, X. Li, C. Liu, S. Adimi, S. Wen, Y. Xu, Oxygen vacancies dominated CuO@ZnFe₂O₄ yolk-shell microspheres for robust and selective detection of xylene, *Sens. Actuators B Chem.* 295 (2019) 117–126.
- [41] H. Cheng, M. Li, C. Su, N. Li, Z. Liu, Cu-Co bimetallic oxide quantum dot decorated nitrogen-doped carbon nanotubes: a high-efficiency bifunctional oxygen electrode for Zn-air batteries, *Adv. Funct. Mater.* 27 (2017) 1701833.
- [42] J. Zhou, Y. Dou, A. Zhou, L. Shu, Y. Chen, J. Li, Layered metal-organic framework-derived metal oxide/carbon nanosheet arrays for catalyzing the oxygen evolution reaction, *ACS Energy Lett.* 3 (2018) 1655–1661.
- [43] L. Xu, X. Wang, L. Chai, T. Li, Y. Hu, J. Qian, S. Huang, Co₃O₄-anchored MWCNTs network derived from metal-organic frameworks as efficient OER electrocatalysts, *Mater. Lett.* 248 (2019) 181–184.
- [44] Y. Qin, J. Yuan, J. Li, D. Chen, Y. Kong, F. Chu, Y. Tao, M. Liu, Crosslinking graphene oxide into robust 3D porous N-doped graphene, *Adv. Mater.* 27 (2015) 5171–5175.
- [45] Y. Zhao, J. Zhang, X. Guo, H. Fan, W. Wu, H. Liu, G. Wang, Fe₃C@nitrogen doped CNT arrays aligned on nitrogen functionalized carbon nanofibers as highly efficient catalysts for the oxygen evolution reaction, *J. Mater. Chem. A* 5 (2017) 19672–19679.
- [46] B. Coasne, Multiscale adsorption and transport in hierarchical porous materials, *New J. Chem.* 40 (2016) 4078–4094.
- [47] L. Wu, Q. Li, C. Wu, H. Zhu, A. Mendoza-Garcia, B. Shen, J. Guo, S. Sun, Stable cobalt nanoparticles and their monolayer array as an efficient electrocatalyst for oxygen evolution reaction, *J. Am. Chem. Soc.* 137 (2015) 7071–7074.
- [48] Y. Tu, P. Ren, D. Deng, X. Bao, Structural and electronic optimization of graphene encapsulating binary metal for highly efficient water oxidation, *Nano Energy* 52 (2018) 494–500.